



Shrinkage of blended cement concrete with fly ash or limestone calcined clay

Sumaiya Afroz · Yingda Zhang · Quang Dieu Nguyen · Taehwan Kim · Arnaud Castel

Received: 1 June 2022 / Accepted: 1 January 2023 / Published online: 13 January 2023
© The Author(s) 2023, corrected publication 2023

Abstract This study investigates the shrinkage of two sustainable aluminosilicate blends with fly ash or limestone-calcined clay (LC3). Paste and concrete were prepared using these SCMs for the highest possible replacement of binder without compromising the strength. The chemical and autogenous shrinkage were assessed for paste samples and further investigation were conducted on hydration by thermogravimetric analysis (TGA) and Fourier transform infrared spectroscopy (FTIR). Opting for an engineering approach, comparison among different segments of shrinkage i.e., autogenous, drying and total shrinkage of concrete having a specific compressive strength were considered. The initial investigation on paste samples highlighted the dissimilarities in shrinkage and hydration of fly ash and calcined clay. LC3 hydrated faster compared to fly ash leading to greater autogenous shrinkage. The high autogenous shrinkage in the LC3 blend was compensated by a low drying shrinkage for a specific compressive strength. Considering the replacement level of cement, shrinkage,

and ecological impact, LC3 proved to be a more sustainable and eco-friendly concrete compared to fly ash.

Keywords Shrinkage · Fly ash · Limestone-calcined clay cement (LC3) · Strength-based approach

1 Introduction

Though concrete is not mandatory for human survival, it is the second most-consumed substance in the world having a per capita consumption of two cubic meters annually [1, 2]. It is the most popular building material due to its versatility and durability. Typically, concrete is composed of 10–15% of Portland cement (PC). Paste, which is the mixture of Portland cement (PC) and water, is the main component of concrete to impact the mechanical and durability performance including shrinkage. The production of clinker in cement is associated with CO₂ emissions due to the thermal decomposition of limestone (raw material) and associated combustion of fossil fuel to produce the required energy [3]. Even the highest maximum thermodynamically possible efficiency in the modern kiln was unable to reduce the emission and energy consumption [4]. In 2020 alone, the estimated worldwide cement production was 4.1 giga metric tons (Gt) [5] and this accounts for 5–8% anthropogenic CO₂ emissions and 90% of industrial CO₂ emission

S. Afroz (✉) · Y. Zhang · T. Kim
School of Civil and Environmental Engineering,
University of New South Wales, Sydney,
NSW 2052, Australia
e-mail: s.afroz@unsw.edu.au

Q. D. Nguyen · A. Castel
School of Civil and Environmental Engineering,
University of Technology Sydney (UTS), Sydney,
NSW 2007, Australia



[3, 6–9]. One of the most promising ways to reduce clinker production and subsequent CO₂ emissions is to use Supplementary Cementitious Materials (SCMs) to replace Portland cement (PC) in concrete [10]. In addition, using SCMs as PC replacement leads to economical and durable concrete in the long run and further contributes to a sustainable environment by utilizing industrial waste or by-products [11].

Aluminosilicates such as fly ash have been used as SCMs in the concrete industry for decades. Fly ash is the by-product of pulverized coal combustion in the thermal power plant which is essentially the most polluting means for the generation of electricity. Moreover, fly ash itself can cause various environmental problems if handled improperly during construction [12, 13]. Despite the environmental issues, fly ash has been used as a replacement for PC due to its pozzolanic reactivity [14–17]. However as reported in 2018, only 10% of the total cement demand for concrete around the world can be replaced by good quality fly ash [2, 18]. Additionally in recent times, the coal-based power plants are being shut down and the production of fly ash is reducing. Other conventional SCMs like slag also has less supply not meeting the demand [18]. These factors acted as a driving force to consider the introduction of new materials and one of the promising cements is the ternary blend of cement with limestone and calcined clay (LC3).

Both limestone and calcined clay are abundantly available making the blend one of the most economical and desirable options [2, 18]. Calcined clay is produced by igniting kaolinite rich clays at 700–850 °C as opposed to the high temperature (1450 °C) required for clinker production [18–20]. Moreover, the calcination of the clays does not involve the CO₂ emission due to the decarbonization of limestone in the cement kiln. Thus, LC3 is a sustainable and environmentally friendly cement that significantly reduce clinker usage and replace other SCMs such as fly ash and slag.

Both fly ash and calcined clay are aluminosilicates having similar chemical compositions and reaction mechanisms. Low calcium fly ash is mainly pozzolanic only, which is similar to calcined clay [21, 22]. Fly ash shows a late pozzolanic effect and reacts with calcium hydroxide to form C-(A)-S-H [23, 24]. Similarly, calcined clay is a pozzolan, but it is reported to react at an early age [18, 25]. Moreover, in a LC3 mix, the limestone can also react and produce mono and/or

hemicarboaluminate [26, 27]. There is a synergy between calcined clay and limestone enhancing each other's reactivity [25, 28]. Therefore, the commencement of reaction in the two aluminosilicates, i.e. fly ash and calcined clay is different and that can influence the subsequent degree of hydration and other related parameters.

Shrinkage is one of the mechanical behaviour of concrete closely related to the mineral admixture used, their proportion to cement, the fineness of the binders and curing [29–31]. The shrinkage (in other words, the total shrinkage) is a combination of chemical, autogenous and drying shrinkage each of which dominate different ages of hydration. While chemical shrinkage is entirely associated with the hydration reactions, the autogenous shrinkage is also influenced by hydration induced self-desiccation [32–35]. The drying shrinkage occurs due to the physical loss of water from the pores of hardened concrete [36]. While shrinkage is well correlated with the concrete mix design, it is often estimated based on the compressive strength. For practical purposes, the knowledge of the extent of shrinkage development for a particular strength grade of concrete is vital for the selection of appropriate materials. In this study, an engineering approach was considered to evaluate two different strength grades for fly ash and LC3.

The replacement level of the SCMs significantly influences the hydration and all related parameters of the cementitious system. On the other hand, to achieve the goal to produce sustainable concrete, the highest possible replacement level is desired. However, this highest feasible replacement level depends on the material type and comparable mechanical properties. Between fly ash and LC3 blends, fly ash blends show low early strength and LC3 blends can achieve satisfactory strength from an early age due to the synergy between the calcined clay and limestone [37–40]. As much as 50% fly ash has been reported in high-volume fly ash mixes [41]. However, Singh and Garg [42] used 25% fly ash replacement in ordinary concrete without sacrificing any mechanical strength. For LC3 concrete since 2012 following Antoni et al. [37], 45%–50% replacement by calcined clay and limestone at a ratio of 2:1 is the most popular mix design [25, 28, 43–49]. In this study, the highest possible replacement levels were selected for respective SCMs based on literature.



This paper aims to advance knowledge that facilitates the selection of suitable aluminosilicate as a cement replacement in sustainable concrete for a specific target strength in term of shrinkage. Shrinkage largely governs the risk of early age concrete cracking [49, 50] which is one of the major barriers for new concrete technology adoption by the industry. Though the shrinkage of fly ash blends were extensively investigated [51–56], very little data on the shrinkage of LC3 mixes available [45, 57]. Moreover, the effect of the early commencement of limestone-calcined clay reaction on shrinkage was not explored previously in comparison to the pozzolanic effect of fly ash. In this study, two aluminosilicate blends with high amounts of respective SCMs i.e., 30% replacement by fly ash and 44% replacement by calcined clay and limestone were investigated and their shrinkage was compared in light of the difference in their hydration. Firstly, the general trend of autogenous shrinkage was identified on paste samples. Secondly, the shrinkage was explained by analyzing the hydration. Finally, the shrinkage and ecological impact of concrete samples with 30% fly ash and 44% LC3 having 25 MPa and 32 MPa compressive strength were compared.

2 Materials and mix design

2.1 Materials

In this study, two types of aluminosilicate blends were investigated. The binders used were General Purpose

(GP) cement, two aluminosilicates i) fly ash and ii) calcined clay and limestone. Table 1 presents the oxide compositions of the binders obtained by wavelength-dispersive X-ray fluorescence (WD-XRF). General Purpose (GP) cement can contain up to 7.5% mineral additives including limestone in accordance with AS 3972 [58]. The fly ash (Blue Circle fly ash) was supplied by Boral Cement. This fly ash had a combined amount of SiO₂, Al₂O₃ and Fe₂O₃ exceeding 50% and CaO less than 18% (see Table 1) and thus conformed with the chemical composition criteria of Class F fly ash in ASTM C618 [59]. The calcined clay was produced by the rotary kiln method and was readily available. The calcined kaolinite content of the calcined clay was estimated using R3 calorimetry test [28] and that content was approximately 47.5% (Afroz et al., unpublished results [60]). Omya Australia supplied the limestone under the commercial name of Omyacarb. The mineralogical phases present in the raw materials were quantified by Rietveld analysis of X-ray diffraction (XRD) patterns and silicon was used as the external standard. To ensure adequate intensity to noise ratio for Rietveld analysis, the X-ray diffraction (XRD) patterns were collected with a PANalytical X'Pert diffractometer (CuK α radiation, $\lambda = 1.54 \text{ \AA}$) with the following settings: range of scanning of 5° to 70° 2 θ , scan rate at 0.0839 deg/sec and step size of 0.0131°. From the phase composition in Table 2, the amorphous content of fly ash and calcined clay were 85.6% and 84.0% respectively. The amorphous content of calcined clay is higher than the estimated kaolinite content (47.5%) before the calcination. This

Table 1 Chemical composition of binders

Chemical composition	Contents %			
	Cement	Fly ash	Calcined clay	Limestone
Silicon dioxide, SiO ₂	18.96	64.01	51.22	1.10
Aluminium oxide, Al ₂ O ₃	4.81	24.75	39.37	0.24
Ferric oxide, Fe ₂ O ₃	3.14	2.87	2.56	0.17
CALCIUM oxide, CaO	63.76	1.63	0.18	54.84
magnesium, MgO	1.20	0.57	0.10	1.53
Sulfur trioxide, SO ₃	2.37	0.10	0.02	0.03
Sodium oxide, Na ₂ O	0.21	0.75	0.20	0.04
Phosphorus pentoxide, P ₂ O ₅	0.08	0.11	0.08	< 0.01
Potassium oxide, K ₂ O	0.46	2.24	0.09	0.01
Titanium dioxide, TiO ₂	0.22	0.95	2.88	< 0.01
Loss on ignition	3.96	1.03	2.19	43.11

Table 2 Phase composition (%) of cement and aluminosilicates

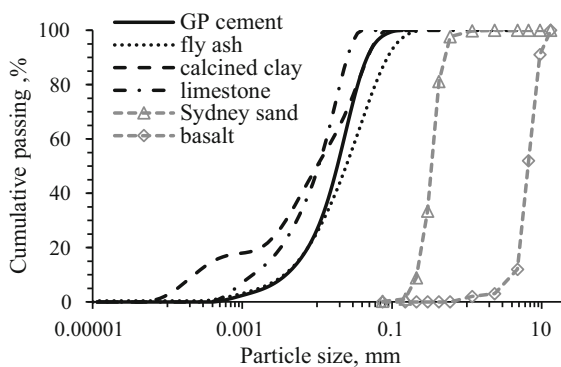
Cement	Fly ash		Calcined clay		
Tricalcium silicate, C ₃ S	51.2	Quartz	11.8	Kaolinite	8.7
Dicalcium silicate, C ₂ S	16.5	Mullite	2.6	Mullite	4.5
Tricalcium aluminate, C ₃ A	6.5	Hematite	0.13	Anatase	1.2
Tetracalcium aluminoferrite, C ₄ AF	7.3			Quartz	1.1
Gypsum	0.9			Rutile	0.4
Bassanite	0.6				
Calcite	5.2				
Amorphous	11.7	Amorphous	85.6	Amorphous	84.0

may be due to: i) the error of the estimation using R3 calorimetry test [28], ii) the additional amorphous content in the calcined clay [22], iii) the formation of glassy silica during cooling after the calcination [61]. The particle size distribution of the raw binders was determined by a laser diffraction particle size analyzer (Malvern Mastersizer 2000) and is presented in Fig. 1. The fly ash was coarser and both calcined clay and limestone were finer than the GP cement.

For concrete, Sydney sand and 10 mm basalt were used as fine and coarse aggregate. The Sydney sand had specific gravity and water absorption of 2.65 and 3.50% respectively. The basalt aggregate had specific gravity and water absorption of 2.80 and 1.08% respectively. The particle size distribution of fine and coarse aggregate by sieve analysis [62] is presented in Fig. 1.

2.2 Sample preparation

Three paste mixes were prepared with a water to binder ratio of 0.4, i) control with no replacement of GP cement, ii) 30F with 30% replacement by fly ash

**Fig. 1** Particle size distributions of binders

and iii) 44L with 44% replacement by calcined clay and limestone. In 44L, the ratio of added 44% calcined clay and limestone was 2 to 1. However, the GP cement was assumed to have about 6% limestone (5.2% calcite from Table 2) which essentially resulted in about 50% clinker content in 44L. No gypsum optimization was carried out for any of the mixes to investigate the effect of direct replacement by SCMs on cementitious systems.

The paste was mixed according to ASTM C305 [63] and three types of samples were prepared for, i) chemical shrinkage, ii) autogenous shrinkage and iii) microstructural analysis. The details about the shrinkage sample preparation will be described in Sect. 3.2. For the preparation of microstructural analysis samples, the paste after mixing was poured into cylindrical plastic containers having 50 mm diameter and 100 mm height. The containers were sealed with plastic lids and covered with parafilm. The prepared samples were cured inside an environmental chamber at 23 °C till testing.

Three mortar mixes were prepared to determine the compressive strengths of the blends. These companion mortar mixes had identical binder components (no replacement, 30% fly ash and 44% calcined clay and limestone) and water-to-binder ratio (0.4) of to the paste mixes and termed as i) control-M, ii) 30F-M and iii) 44L-M. The mortar samples were mixed according to ASTM C305 [63] with a binder to fine aggregate ratio of 1:1. Mortar cubes (50 × 50 × 50 mm) were casted, demolded at 24 h, and cured under water in a temperature-controlled room at 23 ± 2 °C till testing.

A total of six concrete mixes were prepared with different binders having the same replacement levels as the paste samples corresponding to each binder. Two strength categories were considered, (i) 25 MPa and (ii) 32 MPa. Concrete mix designs are given in

Table 3 Mix proportions of concrete

Mix	Mix proportions by weight (kg/m ³)								28 days compressive strength, MPa
	Cement	fly ash	Calcined clay	Lime-stone	Binder	Coarse aggregate	Fine aggregate	Water to binder	
N25-0	310	0	0	0	310	1059	866	0.56	30.7 ± 1.05
N25-FA30	215	95	0	0	310	1071	876	0.46	25.1 ± 1.37
N25-LC44	173.6	0	93	43.4	310	1046	856	0.56	31.0 ± 0.91
N32-0	360	0	0	0	360	1025	839	0.49	32.5 ± 1.26
N32-FA30	250	110	0	0	360	1043	853	0.40	33.5 ± 1.15
N32-LC44	201.6	0	108	50.4	360	1010	826.5	0.49	38.4 ± 1.43

Table 3. This study investigated 25 MPa and 32 MPa concrete (relatively low strength grades) to minimize the effect of the superplasticizer while having a high degree of hydration reactions and because 25 MPa and 32 MPa are the most used concrete grades in practice which means potentially to highest embodied carbon savings. As the water-to-binder ratios were high in this study for low grade concrete, adequate hydration reactions of the binders were ensured and thus could be reasonably compared with the paste results.

Before mixing the aggregates, both fine and coarse, were brought to saturated surface dry (SSD) condition. The aggregates were dried for 24 h at 105 °C and after that absorption water corresponding to absorption % was added before 24 h of casting. The binder and the aggregates were mixed in dried condition for 2 min, then water was added, and then the concrete was further mixed for 5 min. Superplasticizer (MasterGlenium SKY 8100; a polycarboxylic ether polymer) was added if necessary at a dose below 0.15% of binder content to ensure negligible effect of superplasticizer on shrinkage [57]. Two types of concrete samples were prepared, i) cylinders (100 mm in diameter and 200 mm in height) and ii) prisms (75 × 75 × 280 mm). After mixing, the samples were covered and kept in a temperature-controlled room at 23 ± 2 °C and relative humidity of 50 ± 3%. All of the samples were demolded after 1 day and cured. The curing conditions of the concrete samples are described in the experimental methods (Sect. 3.5).

3 Experimental methods

3.1 Heat of hydration by isothermal calorimetry

The heat of hydration of paste samples was monitored by isothermal calorimetry. A TAM Air calorimeter from TA instruments was used to monitor the heat evolution according to ASTM C1702 [64] up to 7 days at 23 °C. Approximately 7 g of the paste sample were mixed inside a glass ampule thoroughly. After mixing, the ampoule was sealed with an aluminum cap and placed inside the calorimeter. The corresponding reference sample was prepared using quartz sand. Two replicates were prepared for each mix.

3.2 Shrinkage of paste

Chemical shrinkage specimen was prepared with paste according to a modified version of ASTM C1608 [65] as described by Zhang et al. [66]. Erlenmeyer flask was used instead of small glass vials and the thickness of paste in the flask was maintained at 7–8 mm for all samples [66]. Two replicates were prepared for each mix. The data acquisition was as per ASTM C1608 [65]. Chemical shrinkage was monitored for 170 days, and the temperature of the samples was maintained at 23 ± 2 °C.

The paste was used to prepare the autogenous shrinkage samples in corrugated tubes and three replicates were prepared for each mix. The samples were prepared according to ASTM C1698 [67]. The

plastic corrugated tubes supplied by Germann Instruments was filled with paste and the ends were sealed with caps according to the code. To mitigate the bleed water absorption and subsequent expansion, the samples were rotated at 4 rpm as suggested by Mohr and Hood [68] for 24 h. After 24 h, the samples were stored in an environmental chamber at 23 °C. The first measurement was taken at the final setting time with a horizontal dilatometer; also supplied by Germann Instruments. The final setting time was determined by isothermal calorimetry for each mix according to the method described by a previous study [69]. Initially, the measurements were taken frequently, and the frequency was reduced with time as needed when the shrinkage stabilized.

3.3 Microstructural analysis of paste

At the specific age for the analysis, each paste sample was removed from the cylindrical plastic containers. Then, the cylinders were broken into fragments. Paste samples for attenuated total reflection (ATR) – Fourier transform infrared (FTIR) analysis were prepared using the solvent exchange method to stop the hydration. At predesignated days, some of the fragments were ground with a Fritsch Pulverisette 6 planetary mono mill and the powders were passed through an 850 microns sieve following Snoeck et al. [70]. The powders were immersed in isopropanol (IPA) for hydration stoppage by solvent exchange according to a modified version of RILEM technique [71]. Every 3 g powder were immersed in 100 ml IPA. Though the RILEM technique [71] advised 15 min as the duration of immersion, the powders were treated for 60 min and the solution was stirred with a magnetic stirrer. The powders were vacuum filtered by membrane filter using a Büchner funnel and rinsed twice with diethyl ether. In a recent study, Zhang and Scherer [72] also advised a longer exchange period for proper hydration stoppage. The filtered powder on the membrane filter was dried in a ventilated oven at 40 °C for 30 min. This IPA treatment ensured negligible carbonation of the samples. The dried powder was collected inside plastic vials and stored inside an N₂ atmosphere glove box till testing. ATR–FTIR spectra were collected for the IPA treated powdered samples with a Perkin Elmer Frontier IR spectrophotometer with a 3 mm diameter diamond/ZnSe crystal. Each spectrum of collected for wavenumbers from

4000 to 500 cm⁻¹ with a resolution and accumulation of 2 cm⁻¹ and 32 respectively.

Solvent exchange can cause additional weight loss at high temperatures. As Zhang and Scherer [73] reported, excess thermogravimetric analysis (TGA) weight loss was observed at temperatures higher than 600 °C for samples treated with solvents. Therefore, TGA was carried out using the powdered oven-dried paste samples at 1, 3, 7, 14, 28, 56 and 90 days. The remaining fragments of paste samples were dried in an oven for 24 h and then ground with a Fritsch Pulverisette 6 planetary mono mill. The powders were passed through an 850 microns sieve. The oven-dried powdered samples were also stored inside the N₂ atmosphere glove box. For each test, approximately 30 mg samples were analyzed in an alumina crucible using a Q600 SDT from TA instrument. The temperature was increased from room temperature to 900 °C at 10 °C/min using a nitrogen purge of 50 ml/min.

3.4 Strength of mortar

Compressive strengths of the mortar cubes were measured according to ASTM C109/C109M [74] after 7 and 28 days of moist curing.

3.5 Strength and shrinkage of concrete

Three cylindrical concrete samples were used to determine the compressive strength of each concrete mix according to ASTM C39 [75] at 28 days. Before the test, the samples were moist cured under 23 ± 2 °C for 28 days.

The prism (75 × 75 × 280 mm) samples were used to measure the shrinkage of concrete. The shrinkage was segmented into two parts and the experimental procedure for each part was followed accordingly. For autogenous shrinkage determination, the prism samples were wrapped with an adhesive aluminium tape after demolding to prevent any moisture exchange and stored in a temperature-controlled room at 23 ± 2 °C. The total shrinkage prisms were demolded and directly kept in a temperature-controlled room at 23 ± 2 °C and relative humidity of 50 ± 3%. For all cases, the initial measurement was collected at 24 h on three replicates with a vertical length comparator. After that, subsequent measurements were taken with a short interval at an early age before decreasing the measurement



frequency with stabilization of shrinkage with time up to 100 days.

4 Results and discussion

4.1 Compressive strength

The compressive strengths of two sets of concrete mixes showed at least 25 MPa and 32 MPa respectively (Table 3) which were used as a basis of separation into two groups. The authors acknowledge the limitations of the mix design of the blended mixes.

Compressive strength of mortar mixes showed the effects of fly ash and limestone-calcined clay inclusion on strength development (Table 4) which is closely related to the hydration process. At 7 and 28 days, control-M exhibited the highest compressive strength followed by 44L-M and 30F-M respectively. Even with 56% replacement of GP cement, 44L-M performed better compared to 30F-M regarding strength development. At 28 days, the compressive strength of 44L-M was similar to control-M.

4.2 Shrinkage of paste

4.2.1 Chemical shrinkage and heat of hydration

Chemical shrinkage is the reduction in absolute volume of paste due to hydration as the volume of the products are less than that of the reactants [35]. Chemical shrinkage describes the earliest deformation in cement paste immediately after mixing. Calcined clay has been reported to react as early as 24 h [25]. Although the class F fly ash does not participate to the early age hydration and initially act as a filler [76], the chemical shrinkage was considered with respect to the binder content instead of cement content to account for

any possible pozzolanic reaction of calcined clay. Similar to chemical shrinkage, the heat of hydration of cementitious materials are often used to estimate the rate of hydration at a very early age. This section presents the chemical shrinkage and heat of hydration of the different paste systems and their interrelation.

Figure 2a presents the chemical shrinkage of paste with respect to the binder content up to 170 days. The control mix showed a plateau after about 50 days. The chemical shrinkage of the 30F sample was the lowest up to 20 days and after that, it continued to increase with a slow rate, indicating the late pozzolanic behaviour. The chemical shrinkage of the 30F seems to surpass that of control at 84 days. The chemical shrinkage of 44L increased faster than that of 30F for up to about 20 days (see Fig. 2a and b). However, it reached a plateau at about 20 days and then showed the lowest chemical shrinkage at the end of the measurement period.

Figure 2b plots both chemical shrinkage (dashed lines) and heat of hydration (solid lines) at an early age and highlights that the chemical shrinkage correlates with the early age hydration for the three different paste mixes. As shown in Fig. 2b, the overall trends of chemical shrinkage development over 7 days were very similar to the corresponding trends of the cumulative heat of hydration evolution. However the order of heat of hydration (control > 44L > 30F) did not match the order of the chemical shrinkage (44L > control > 30F) for 7 days of hydration. At the early hydration period (up to 7 days), the chemical shrinkage of the 44L paste was comparable to or slightly higher than that of the control paste (Fig. 2b). Control and 44L pastes had higher chemical shrinkage compared to 30F paste although 44L pastes had less amount of GP (56% of binder) than 30F (70% of binder).

It is also interesting to note that for 12 h, the heat of hydration of the 44L paste was almost identical to that of the control despite 56% of GP cement replacement. The filler effect and the increased effective w/c due to the addition of limestone and calcined clay could play a significant role in the hydration rate and compensate for the dilution effect (due to less amount of GP cement in 44L than in the control paste). However, these two effects that accelerate the hydration of GP cement could also be valid for the case of the 30F paste but 30F exhibited less heat of hydration. This strongly indicated the participation of the early hydration

Table 4 Compressive strengths of mortar

Mix	Compressive strength, MPa	
	7 days	28 days
Control-M	35 ± 0.64	40.5 ± 1.27
30F-M	27.2 ± 0.38	35.4 ± 0.83
44L-M	32.6 ± 1.28	39.6 ± 1.13

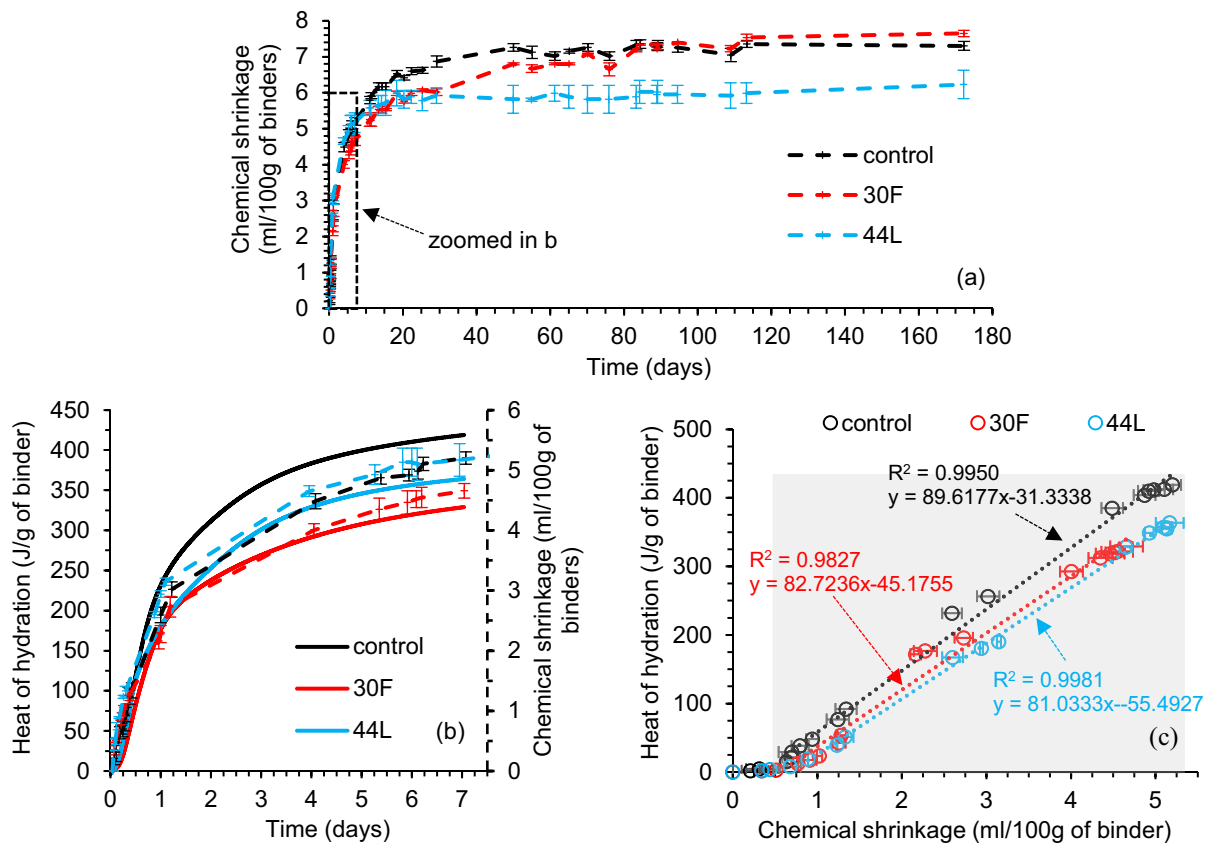


Fig. 2 **a** Chemical shrinkage (dashed lines) up to 170 days, **b** Chemical shrinkage and heat of hydration (solid lines) up to 7 days and **c** Relation between chemical shrinkage and heat of hydration of paste samples up to 7 days

reaction of limestone and calcined clay in 44L paste. For 12 h of the very early hydration, the chemical shrinkages of 30F and 44L were slightly higher than that of the control sample.

The above observations confirmed that limestone-calcined clay blend in 44L paste caused faster initial hydration reactions than the fly ash blended cement did. The combined effects of early filler effect and early pozzolanic reaction in 44L mix led to the highest chemical shrinkage till 20 days hydration, which was also supported by the TGA results to be discussed in Sect. 4.3.2. However, 44L showed the lowest chemical shrinkage after 20 days compared to the other mixes indicating the absolute volume change due to hydration had a minor influence on the shrinkage of 44L paste at later ages. The rate of early age chemical shrinkage development has the potential to influence the early-age autogenous shrinkage of the paste and will be discussed in Sect. 4.2.2.

After the initial accelerated hydration (up to 0.2 days or about 5 h), the heat of hydration and chemical shrinkage varied almost linearly for all mixes up to 7 days (Fig. 2c). The slope of the linear part (shaded in Fig. 2c) were 8.96, 8.27 and 8.10 kJ/ml for control, 30F, and 44L respectively. A lower value of the slope indicates that less heat was produced to achieve a similar extent of chemical shrinkage for blended mixes. This may be the result of different hydration products or reactions involved in the hydration of pozzolanic materials.

4.2.2 Autogenous shrinkage

The autogenous shrinkage is closely related to the hydration reactions because it is partly generated by chemical shrinkage. During the hydration process, the relative humidity in the capillary pores in pastes reduces causing self-desiccation. The self-desiccation produces stresses on the pore walls and subsequent

macro shrinkage. This shrinkage due to self-desiccation contributes significantly to the autogenous shrinkage [32–34]. In addition, the time-dependent refinement of the pore structure can further increase autogenous shrinkage [77–80].

The autogenous shrinkage of paste samples was monitored for up to 200 days and the results are presented in Fig. 3a. To compare the performance of 30F and 44L samples with the control sample, Fig. 3b shows the percentages of autogenous shrinkage of 30F and 44L based on that of the control sample at each day.

The autogenous shrinkage was higher for both 30F and 44L samples at 1 day compared to the control sample (Fig. 3a and b). This may be associated with the accelerated initial hydration of 30F and 44L samples, as seen from chemical shrinkage results (Fig. 2b) because the high chemical shrinkage originating from rapid hydration can cause both high self-desiccation and high autogenous shrinkage. In fact, the autogenous shrinkage of 44L at 1 day was about 3 times higher than that of control (5.4%). Due to the filler effect and the increased effective w/c in 44L

explained in Sect. 4.2.1, the pore structure for LC3 mix (i.e. 44L) was expected to be more refined even at a very early age, which was also reported in several studies [37, 81, 82]. The combined effect of the faster hydration and finer pore structure seems to cause the higher autogenous shrinkage than those observed from both control and 30F at 1 day of autogenous shrinkage.

After 1 day, the autogenous shrinkage of 30F was significantly lower than that of the control sample up to 7 days. In previous studies, fly ash blends also showed a lower autogenous shrinkage compared to other binders [51, 78]. However, Termkhajornkit et al. [51] stated that the reduction in autogenous shrinkage with fly ash was strongly dependent on the replacement level. After 7 days, their relative differences started to diminish (Fig. 3b) when compared with the autogenous shrinkage of the control sample. This indicates that the rate of autogenous shrinkage development of 30F after 7 days was greater than for control sample. A possible explanation for the increasing rate of autogenous shrinkage development in 30F after 7 days can be the onset of slow pozzolanic reaction of fly ash causing further hydration and subsequent self-desiccation.

Unlike 30F, the autogenous shrinkage of 44L sample was higher than that of the control sample during the entire monitoring period (Fig. 3a). After 7 days the rate of autogenous shrinkage development of 44L was similar to that of control (see Fig. 3b). Thus, the relative autogenous shrinkage of 44L relative to that of the control sample varied within the range of 143% to 155.5% after 7 days (see Fig. 3b). Previous works on LC3 autogenous shrinkage were contradictory reporting both decrease [46, 83] and increase [84].

In this study, autogenous shrinkage was the highest for 44L and the lowest for 30F samples. The different hydration mechanisms of the two different aluminosilicate binders seemed to influence the autogenous shrinkage differently. The hydration of calcined clay and fly ash will be investigated in Sect. 4.3 and correlated with their shrinkage behaviour.

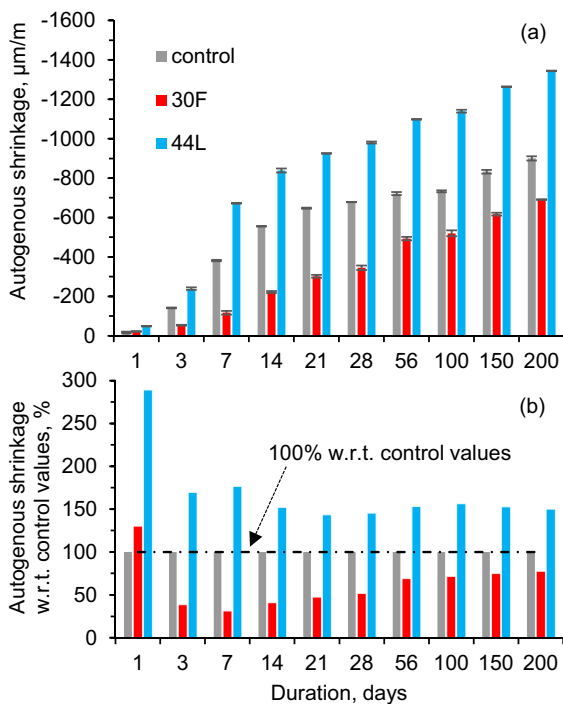


Fig. 3 Autogenous shrinkage of **a** Paste samples and **b** Autogenous shrinkage % with respect to shrinkage of control specimen at each respective day

4.3 Microstructural properties

4.3.1 Evolution of chemical bonding structure (FTIR)

The presence of different raw materials and hydration products were observed by FTIR at 1, 3, 7, 14 and 28 days. Figure 4 presents several distinct peaks over a range of wavenumbers and the peaks indicate absorbance intensities. For solid samples, the absorbance intensity can be influenced by the pressure applied by the ATR unit and the particle size of the sample [85, 86]. The ground samples were sieved thus the particle sizes of the samples can be considered similar for all samples. Identical pressure was applied each time during spectra collection. Therefore, the absorbances of different samples can be considered free from these limitations and comparable. For the identification of the peaks of interest, the spectra were considered between the wavenumbers of $3700\text{--}3600\text{ cm}^{-1}$ and $1050\text{--}850\text{ cm}^{-1}$. Figure 4a1, a2 and a3 feature the peaks corresponding to calcium hydroxide (CH) at about 3644 cm^{-1} wavenumber due to stretching vibration of O—H [87–89] of control,

30F, and 44L respectively. This study is also interested in two other peaks shown in Fig. 4b1, b2, and b3. The peak located at around 950 cm^{-1} due to Si—O stretching indicates the main hydration product C—S—H [87] and the peak around 874 cm^{-1} wavenumber was due to the bending (ν_2) of CO_3^{2-} present in limestone [88, 90, 91].

The calcium hydroxide produced by the hydraulic reaction of the clinker in the blended mixes, 30F and 44L, was lower compared to control because of the dilution effect, also seen in previous studies [92, 93]. Fly ash reacted at later ages producing hydration products and consuming calcium hydroxide [23, 24]. The process starts as the amorphous silica and alumina from fly ash dissolve in the pore solution with high pH [24]. Therefore, the commencement and the extent of the pozzolanic reaction of fly ash depends on the reactivity of the fly ash and the availability of calcium hydroxide from the hydraulic reactions of clinker [93, 94]. From Fig. 4a2, the CH peak for 30F started to diminish slowly at around 14 days when the pozzolanic effect started. On the other hand, for 44L, the pozzolanic effect commenced from day 3 as seen from

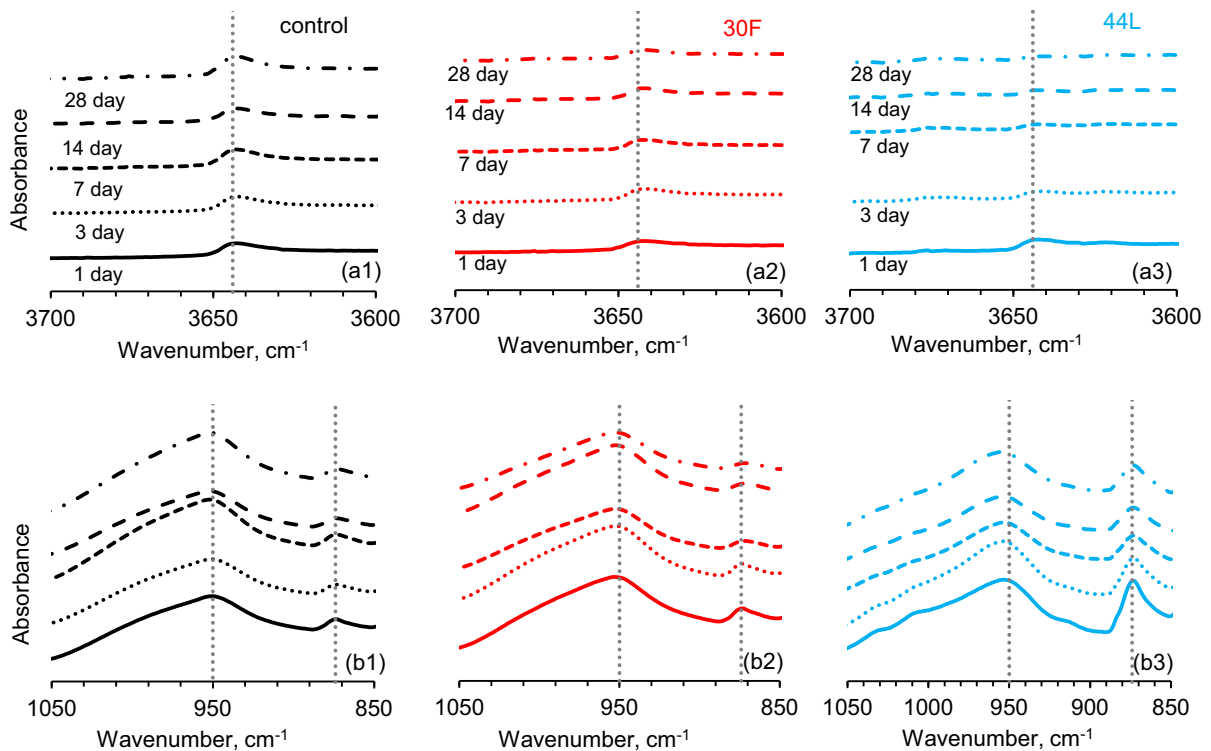


Fig. 4 FTIR spectra of paste samples between wavenumbers of **a** $3700\text{--}3600\text{ cm}^{-1}$ and **b** $1050\text{--}850\text{ cm}^{-1}$



the reduction in the CH peak in Fig. 4a3. The pozzolanic reaction of fly ash and calcined clay was also supported by the TGA data in Sect. 4.3.2. The pozzolanic effect was so intense that the CH peak at 28 days for 44L had minute absorption intensity. Calcined clay has high early pozzolanic behaviour which is well supported by previous studies [18, 20, 28]. The limestone present in the LC3 mix i.e., 44L can further promote the consumption of CH as CH can participate in the formation of carboaluminates from limestone reaction [95].

The calcium carbonate in limestone reacts with alumina to produce mono and hemi carboaluminate [26, 27]. As seen in Fig. 4b2 and b3, the calcium carbonate peak at around 874 cm^{-1} in both 30F and 44L samples showed a diminishing trend. The peak in 30F seems to start to decrease at around 28 days whereas this peak in 44L started to reduce significantly from 3 days, indicating the reaction of limestone. In 44L, the presence of excess alumina from calcined clay could accelerate the limestone reaction [37, 83]. Though 30F mix also had limestone content from GP cement (5.2% as seen from Table 2), the lower amount of the reactive alumina content in fly ash and GP cement than that of calcined clay led to a comparatively very slow reaction of limestone.

The pozzolanic reaction from aluminosilicates produces hydration products refining the pore structure leading to dense microstructure. Moreover, the carboaluminates from limestone reaction can also refine the pore structure [37, 81, 82]. The FTIR results indicated higher pozzolanic and limestone reaction of 44L mix compared to 30F mixes which can lead to finer pore structure and denser microstructure from an early age. The observed increase in autogenous shrinkage in the LC3 mix could be attributed to the finer pore structure produced by the hydration products [96].

4.3.2 Thermogravimetric analysis (TGA)

TGA weight losses of control, 30F and 44L mixes between $105\text{ }^{\circ}\text{C}$ and $900\text{ }^{\circ}\text{C}$ at 1, 3, 7, 14, 28, 56 and 90 days are presented in Fig. 5a1, b1, c1 and the derivative weight loss within a certain temperature range is shown in Fig. 5a2, b2, c2. The percentages of TGA weight loss were based on the total weight of the binder of each mix at $105\text{ }^{\circ}\text{C}$ to avoid the effect of any

residual free water. The weight loss from $105\text{ }^{\circ}\text{C}$ to $400\text{ }^{\circ}\text{C}$ accounted for C-S-H, alumina–ferric oxide–monosulfate (AFm) phases and other minor phases [70, 97, 98]. This provides an indication of the amount of chemically bound water associated with hydration products present in the samples and an indirect measurement of the degree of hydration (DOH) as presented in Fig. 6a. At 3 days, the TGA weight loss % of 30F and 44L between $105\text{ }^{\circ}\text{C}$ to $400\text{ }^{\circ}\text{C}$ were 4.9% and 5.6% respectively. It indicated high reactivity of the LC3 mix (44L) despite having a higher replacement level. At 7 days, the TGA weight loss % of 30F and 44L between $105\text{ }^{\circ}\text{C}$ to $400\text{ }^{\circ}\text{C}$ were 5.8% and 6.5% respectively and both values were higher than that of control (5.4%). The presence of calcined clay and limestone accelerates the hydration at an early age, as early as 24 h, due to the superimposition of filler effect of calcined clay and limestone and pozzolanic effect of calcined clay [25]. Fly ash also promoted the degree of reaction at an early age as reported by Haha et al. [24]. After 7 days, the hydration in 30F mix was the lowest among the three mixes up to 56 days (Fig. 6a). Between 56 and 90 days, the amount of hydration products increased due to the late pozzolanic reaction of fly ash. On the other hand, 44L continued to have a high hydration rate from 7 to 14 days and slowed down after that to almost a constant value between 28 to 90 days.

The weight loss between $400\text{ }^{\circ}\text{C}$ and $500\text{ }^{\circ}\text{C}$ (a slight shift of temperature was observed for control samples at 28, 56 and 90 days) in Fig. 5 were due to the decomposition of calcium hydroxide (CH). The derivative weight losses due to CH decomposition are also illustrated in Fig. 5 a2, b2, c2. The amount of CH per 100 g of anhydrous cement was quantified according to the method described by Kim and Olek [99] and the results are presented in Fig. 6b. For the control samples, the amount of CH gradually increased with time from 1 to 90 days as hydration progressed (Figs. 5 a2 and 6b). The pozzolanic effect was observed for both 30F and 44L samples (Fig. 5b2, c2 and also in Fig. 4). For 30F samples, the amount of CH increased up to 14 days and started to diminish after that (Figs. 5b2 and 6b) indicating pozzolanic action. In the case of 44L, the commencement of the pozzolanic effect was observed earlier. As seen from Figs. 5c2 and 6b, the amount of CH started to decrease after 7 days. Moreover, the reduction of the

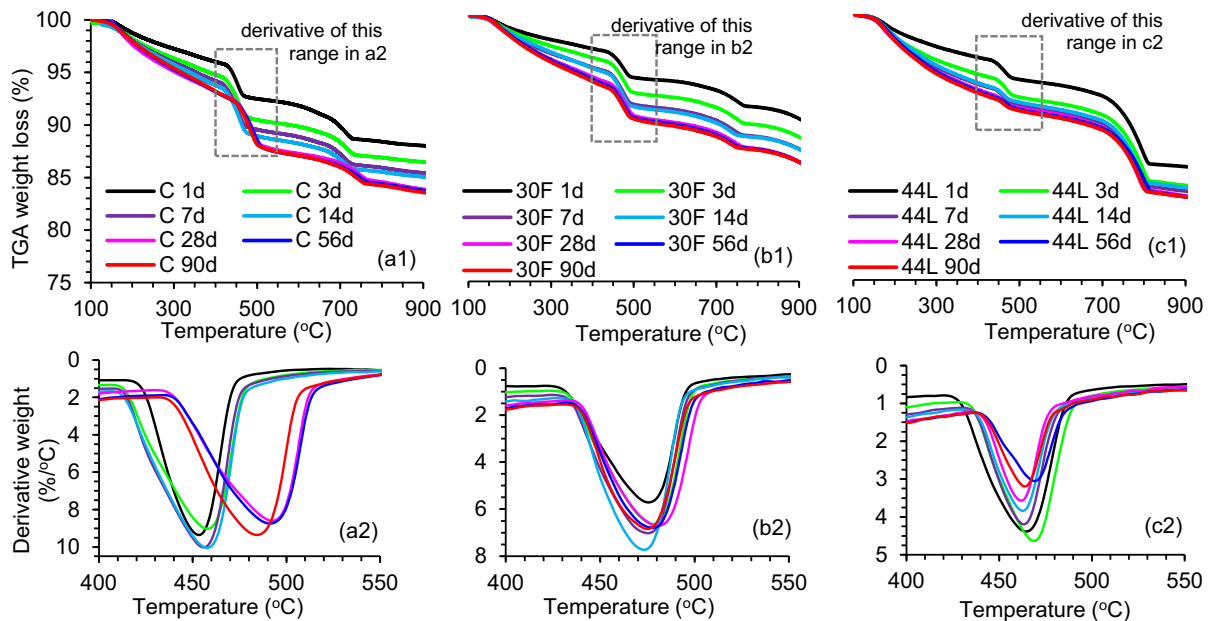


Fig. 5 Total and derivative weight loss of TGA for **a** Control denoted by C, **b** 30% fly ash denoted by 30F and **c** 44% limestone-calcined clay denoted by 44L

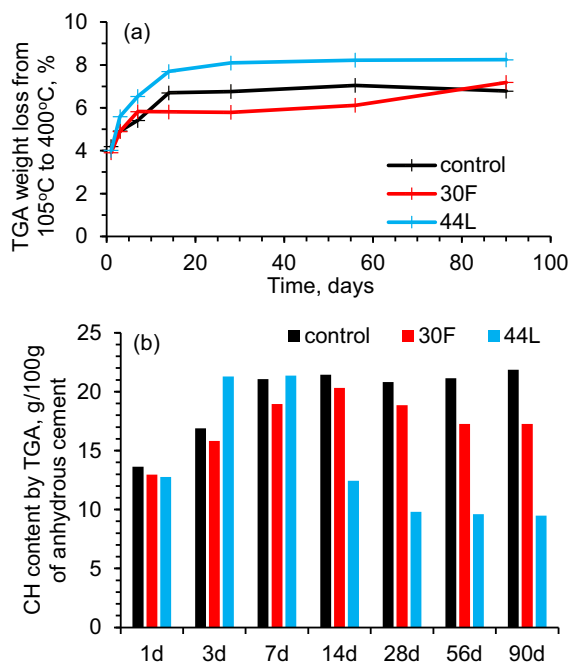


Fig. 6 TGA results **a** Weight loss between 105 and 400 °C and **b** CH (calcium hydroxide) content up to 90 days

amount of CH up to 90 days was considerably high for 44L compared to the fly ash mix. The calcined clay showed very high pozzolanic reactivity as reported previously [18, 20, 28].

The weight loss between 700 and 810 °C in Fig. 5a1, b1, c1 indicated the presence of calcium carbonate [99] from limestone in the cement in the case of control and 30F mixes and the additional limestone for the 44L mix. The calcium carbonate in limestone can react with the excess alumina to produce mono and hemicarboaluminate [26, 27].

The high reactivity of calcined clay promoted the early age hydration and pozzolanic action in 44L mix whereas the pozzolanic effect of fly ash manifested at a later age. Though both of the materials were aluminosilicates in a broader sense, their hydration kinetics were very different. The high hydration rate and high amount of hydration products in 44L compared to 30F influenced the early-age autogenous shrinkage (Fig. 3) by enhancing the extent of pore refinement and self-desiccation.

4.4 Shrinkage of concrete

The investigation on the paste samples confirmed that LC3 mix developed higher autogenous shrinkage compared to the fly ash blended mix though both of the mineral additives were mainly composed of aluminosilicates. From the current study on pastes, the high reactivity of calcined clay can cause this high autogenous shrinkage.

Though concrete shrinkage is impacted by aggregate size, types and their relative proportions compared to paste, it is generally expected to show a similar trend in shrinkage development to that observed in the paste. The high autogenous shrinkage in LC3 paste could lead to high total shrinkage depending on drying shrinkage. In this study, both autogenous shrinkage and total shrinkage of concrete were investigated. The total shrinkage is defined as the overall shrinkage of a specimen exposed to a dry environment.

A grade-based approach is better suited for the practical knowledge about concrete shrinkage. Though shrinkage depends on a number of variables, the overall effect of adding any particular mineral additives is generally assumed to be comparable for mixes with similar compressive strength. However, the grade-based approach rendered the current data incomparable with the previous studies on shrinkage of fly ash based on mix design [51, 53–55]. No data was available for comparison of shrinkage of LC3 with other binders in literature except the work by Dhandapani et al. [45] who followed different curing schemes. The compressive strength of each mix is presented in Table 3.

4.4.1 Autogenous shrinkage of concrete

The autogenous shrinkage of concrete including the two different strength grades considered in this study are presented in Fig. 7. Similar to the autogenous shrinkage of pastes samples (Fig. 3), the autogenous shrinkage of LC3 mixes i.e., N25-LC44 and N32-LC44 was the greatest in their respective strength category as shown in Fig. 7a and b. To facilitate further understanding, the autogenous shrinkage of concrete was expressed with respect to the autogenous shrinkage of the corresponding control specimen at 28 days (bars with a red outline in Fig. 7c). It is important to mention that autogenous shrinkage is significantly influenced by the water to binder ratio [100]. LC3 mixes can provide comparable compressive strength as control mixes formulated with similar water to binder ratio [18]. However, fly ash blended mixes exhibit a lower compressive strength, especially during the early age [101, 102]. Therefore, fly ash blended mixes had a lower water to binder ratio (see Table 3) to achieve the target compressive strength in this study, which influenced the autogenous shrinkage.

As seen in Fig. 7c, autogenous shrinkage of N25-FA30 was higher than the control mix (N25-0) but N32-FA30 was similar to the control mixes (N32-0) though the fly ash concretes was prepared with about 18% less water to binder ratio. On the contrary, the LC3 mixes i.e., N25-LC44 and N32-LC44 showed the highest autogenous shrinkage despite having similar water to binder ratio compared to control (N25-0 and N32-0 respectively). The LC3 concrete result of autogenous shrinkage was also consistent with the observation on the paste samples. For the 25 MPa concrete, the autogenous shrinkage of N25-0, N25-FA30 and N25-LC44 at 100 days was 1.43, 2.87 and 5.06 times higher than that of the benchmark value of 28-day autogenous shrinkage of N25-0 (Fig. 7c). For the 32 MPa concrete, the autogenous shrinkage of N32-0, N32-FA30 and N32-LC44 at 100 days was 1.47, 1.66 and 2.98 times higher than that of the benchmark value of 28-day autogenous shrinkage of N32-0 (Fig. 7c).

The autogenous shrinkage results showed that fly ash blended concrete can be used to minimize the autogenous shrinkage development even with a low water to binder ratio required to achieve the desired compressive strength. In contrast, LC3 mixes produced high autogenous shrinkage despite having the same water to binder ratio as the control mixes. Therefore, depending on the aluminosilicate used, the autogenous shrinkage can vary to a great extent for concretes having similar compressive strength.

4.4.2 Total and drying shrinkage of concrete

Total shrinkage is considered as the superimposition of autogenous shrinkage and drying shrinkage of concrete in this study. The total shrinkage is the ultimate manifestation of shrinkage in practice, used for design purpose. As seen from Fig. 8, the total shrinkage of the aluminosilicate blends was similar to that of the control mixes despite having a high autogenous shrinkage in the case of the LC3 mixes (Fig. 7). For the 25 MPa concretes, the total shrinkage of N25-0, N25-FA30 and N25-LC44 at 100 days was 1.38, 1.44 and 1.34 times higher than that of the benchmark value of 28-day total shrinkage of N25 0 (Fig. 8c). For the 32 MPa concrete, the total shrinkage of N32-0, N32-FA30 and N32-LC44 at 100 days was 1.44, 0.98 and 1.51 times higher than that of the

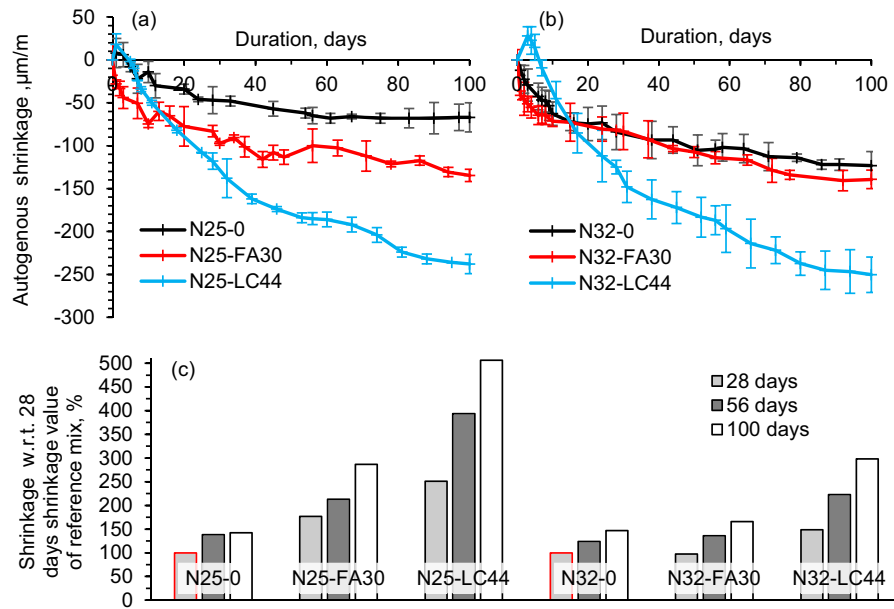
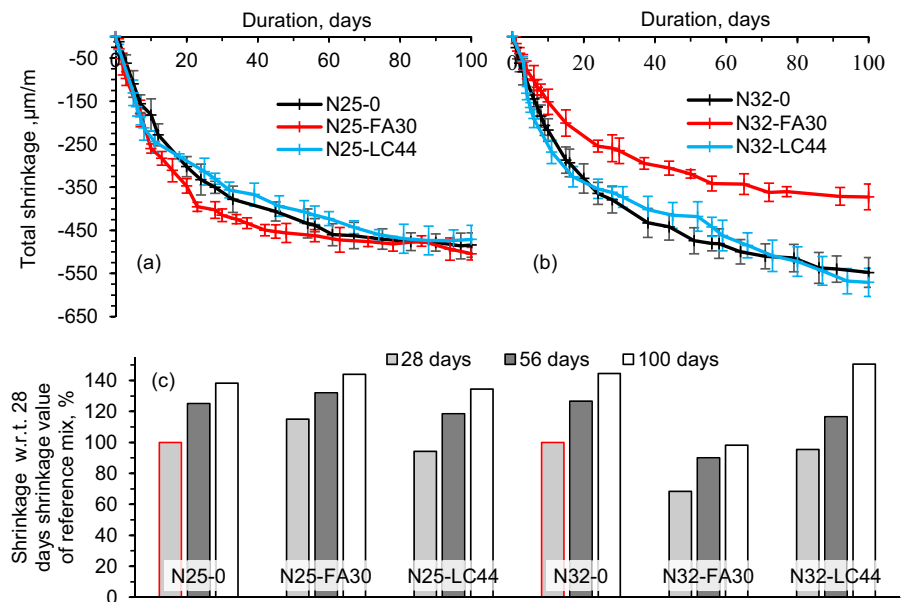


Fig. 7 Autogenous shrinkage of concrete. The bars with red borderlines in **c** Represent the reference shrinkage of each strength grade of concrete (25 MPa and 32 MPa)

Fig. 8 Total shrinkage of concrete. The bars with red borderlines in **c** Represent the reference shrinkage of each strength grade of concrete (25 MPa and 32 MPa)



benchmark value of 28-day total shrinkage of N32-0 (Fig. 8c).

Separation of drying shrinkage from the total shrinkage can provide a possible explanation of the similar total shrinkage for aluminosilicate mixes. In this study, the drying shrinkage was determined by the simplified approach of taking the difference between

total and autogenous shrinkage [57, 103–105]. The results are presented in Fig. 9a and b. However, this simplified method has its limitations. In a total shrinkage specimen, the autogenous shrinkage may reduce as opposed to a completely sealed condition due to the lack of available water for hydration. Therefore, in this paper, this simplified estimation can



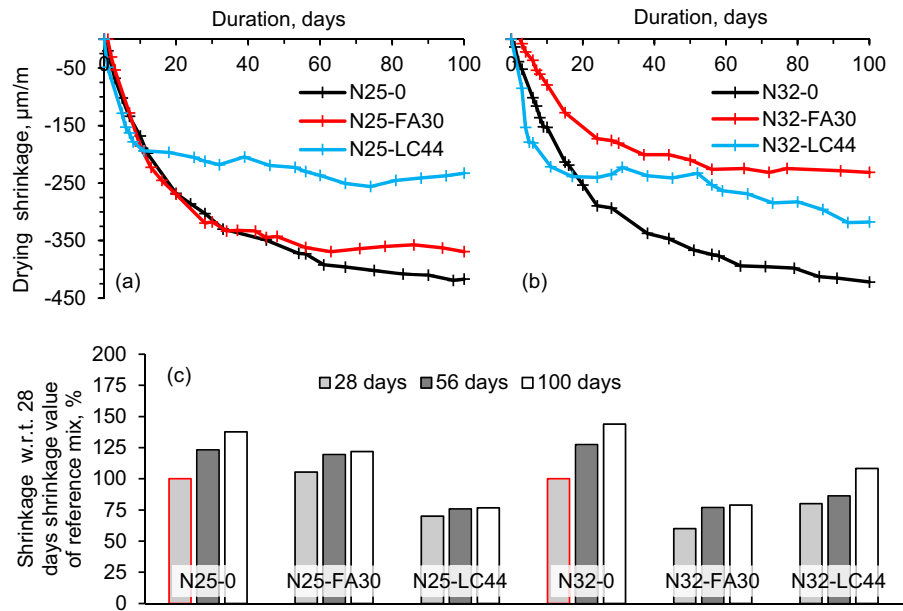


Fig. 9 Drying shrinkage of concrete using a simplified method (total shrinkage – autogenous shrinkage)

only qualitatively indicate the extent of drying shrinkage development. The drying shrinkage of the aluminosilicate blends was similar or lower than that of the control sample. For the 25 MPa concrete, the drying shrinkage of N25-0, N25-FA30 and N25-LC44 at 100 days was 1.38, 1.22 and 0.77 times than that of the benchmark value of 28-day drying shrinkage of N25-0 (Fig. 9c). For the 32 MPa concrete, the drying shrinkage of N32-0, N32-FA30 and N32-LC44 at 100 days was 1.44, 0.79 and 1.08 times higher than that of the benchmark value of 28-day drying shrinkage of N32-0 (Fig. 9c). The drying shrinkage was significantly lower in the case of the LC3 mixes (N25-LC44 and N32-LC44) which compensated for the high autogenous shrinkage resulting in a comparable total shrinkage with the control mixes. The high autogenous shrinkage of the LC3 mixes was compensated by a low drying shrinkage but if the autogenous shrinkage development is substantially high, for example in the case of a very low water to binder ratio, the mitigation effect of the drying shrinkage might be inadequate. For N32-FA30, the water to binder ratio was smaller (0.4) than other concrete mixes and thus less water was available for evaporation, which can explain the low drying shrinkage. Moreover, unreacted fly ash particles act as micro aggregates [15, 51]. This effect could

also decrease the extent of shrinkage, especially at an early age till the late pozzolanic reactions commenced.

5 Ecological evaluation

The ecological impact of the concrete mixes was evaluated by two environmental sustainability indicators, i) CO_2 emission and ii) energy consumption. The results showed that using SCMs to replace the cement content significantly reduced the CO_2 emission and energy consumption (Fig. 10). The estimation of the ecological impact was calculated based on the data presented in Table 5. The embodied carbon represents the total CO_2 associated with the material production and the embodied energy which consists of the total energy required for manufacturing only assuming all aggregates, cement, calcined clay, limestone etc. are available at concrete batching plant. Due to unavailability of data, the embodied carbon and energy per unit of GP cement was assumed to be equal to Portland cement from literature. However, these values should be lower in GP cement than Portland cement as GP cement can contain up to 7.5% mineral additions. Though the binder contents ranged between 12.87% to 15.17% for the six concrete mixes (Fig. 10a), majority of the CO_2 emission and energy consumption are

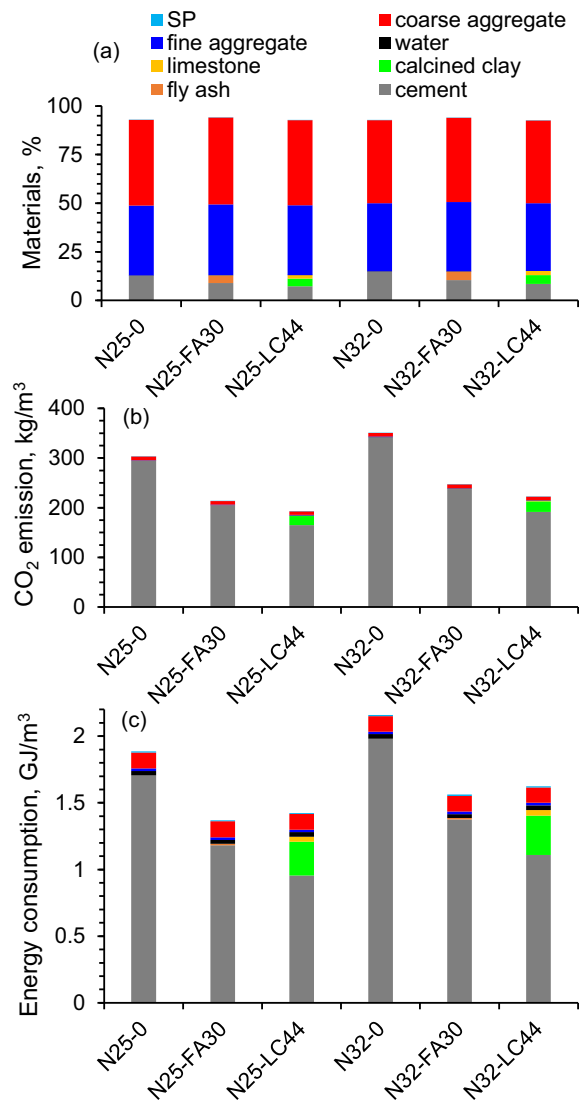


Fig. 10 a Proportions of materials and ecological impact including b CO₂ emission and c Energy consumption of different concrete mixes using the data summarized in Table 5

originated from the binders, especially cement. The CO₂ emission reduced by 29.47% and 51.46% in the case of N25-FA30 and N25-LC44 respectively compared to N25-0 (Fig. 10b). These values were 29.5% and 51.73% for 32 grade concrete. The reduction of energy consumption was about 27% and 34% for 30% fly ash concrete and 44% limestone-calcined clay concrete respectively for both grades (Fig. 10c). The reduction in energy consumption for LC3 was less than that of CO₂ emission due to the calcination process of the clay.

LC3 concrete exhibited excellent performance in terms of these two indicators for environmental sustainability. Limestone and calcined clay are sustainable considering the supply versus the demand. Moreover, a high percentage of cement can be replaced without compromising the early age mechanical strength unlike fly ash. This resulted in the significantly better performance of LC3 compared to fly ash concrete making it a more sustainable and eco-friendly concreting option.

6 Conclusions

This study compared the shrinkage of two aluminosilicate blends i.e., 30% fly ash and 44% limestone-calcined clay (LC3) with a reference mix without any Supplementary Cementitious Materials (SCM) addition. The replacement levels used were very high for the respective SCMs. The investigation was initiated with paste samples to assess shrinkage and microstructural parameters. Finally, the shrinkage of concrete mixes with specified compressive strength i.e., 25 MPa and 32 MPa was examined.

Chemical shrinkage of paste indicated accelerated early age hydration of the LC3 blend compared to the fly ash blend. The autogenous shrinkage was significantly higher for LC3 mixes. While the autogenous shrinkage of the fly ash blend was three-fourths of the control sample at 200 days. The autogenous shrinkage of the LC3 blend was 1.5 times that of control samples. TGA showed that the amount of hydration products (decomposed between 105 to 400 °C) in LC3 mixes was the highest among the three mixes which can be correlated with its highest autogenous shrinkage. The fly ash blend showed a low amount of hydration products till the late pozzolanic reactions commenced. FTIR also corroborated the late pozzolanic reactions in fly ash blend compared to the very fast pozzolanic reactivity of LC3 blends. Moreover, the FTIR analysis confirmed the significant reactions involving limestone in LC3 blends, unlike fly ash blends. The early pozzolanic reaction and limestone reaction in LC3 blends are expected to produce a very fine pore structure. The fine pore structure coupled with a high degree of hydration in LC3 mixes produced a high autogenous shrinkage compared to the fly ash blend.

LC3 concrete autogenous shrinkage was also the highest compared to other mixes, which was

Table 5 Embodied carbon and energy of materials

Material	Embodied carbon (kg eq. CO ₂ /kg)	Embodied energy (MJ/kg)	Data source
Cement	0.9500	5.500	[106]
Fly ash	0.0088	0.110	[107]
Calcined clay	0.1960	2.734	[106]
Limestone	0.0320	0.850	[106]
Water	0.0008	0.200	[106]
Fine aggregate	0.0010	0.022	[108]
Coarse aggregate	0.0070	0.113	[108]
Superplasticizer (SP)	0.7200	18.30	[108]

consistent with the results obtained from the paste samples. Due to the compensating effect of low drying shrinkage, the total shrinkage of the control and LC3 mixes were similar for the two compressive strength grades. The fly ash mixes having lower water to binder ratio to achieve the target compressive strength, showed similar or lower total shrinkage than other mixes. Considering the replacement level of cement, shrinkage, and ecological impact, LC3 proved to be a more sustainable and eco-friendly concrete compared to fly ash.

This study revealed the effect of different hydration processes in aluminosilicate blends on shrinkage of low strength concrete. Further investigation is required of blended concrete having a wider range of compressive strengths. The variability of the reactivity of the SCMs can also be correlated with the shrinkage development as it is heavily relied on the source of the SCMs.

Acknowledgements This research was funded by CCAA and ARC Linkage project LP170100912 titled “Shrinkage, cracking, self-healing and corrosion in blended cement concrete”. The authors would like to thank the Centre for Infrastructure Engineering and Safety, School of Civil and Environmental Engineering and Mark Wainwright Analytical Centre of University of New South Wales (UNSW), UTS tech lab of University of Technology Sydney for providing technical support.

Funding Open Access funding enabled and organized by CAUL and its Member Institutions.

Declarations

Conflict of interest We wish to confirm that there is no conflict of interest associated with this publication and there has been no significant financial support for this work that could have influenced its outcome.

Open Access This article is licensed under a Creative Commons Attribution 4.0 International License, which permits use, sharing, adaptation, distribution and reproduction in any medium or format, as long as you give appropriate credit to the original author(s) and the source, provide a link to the Creative Commons licence, and indicate if changes were made. The images or other third party material in this article are included in the article’s Creative Commons licence, unless indicated otherwise in a credit line to the material. If material is not included in the article’s Creative Commons licence and your intended use is not permitted by statutory regulation or exceeds the permitted use, you will need to obtain permission directly from the copyright holder. To view a copy of this licence, visit <http://creativecommons.org/licenses/by/4.0/>.

References

- Gagg CR (2014) Cement and concrete as an engineering material: an historic appraisal and case study analysis. *Eng Fail Anal* 40:114–140
- Environment UN, Scrivener KL, John VM, Gartner EM (2018) Eco-efficient cements: potential economically viable solutions for a low-CO₂ cement-based materials industry. *Cem Concr Res* 114:2–26
- Herath C, Gunasekara C, Law DW, Setunge S (2020) Performance of high volume fly ash concrete incorporating additives: a systematic literature review. *Constr Build Mater* 258:120606
- Sharma M, Bishnoi S, Martirena F, Scrivener K (2021) Limestone calcined clay cement and concrete: a state-of-the-art review. *Cem Concr Res* 149:106564
- Summaries MC (2021) Mineral Commodity Summaries; USGS Unnumbered Series. US Geol Surv Reston, VA 200
- Chen C, Habert G, Bouzidi Y, Jullien A (2010) Environmental impact of cement production: detail of the different processes and cement plant variability evaluation. *J Clean Prod* 18:478–485
- Barcelo L, Kline J, Walenta G, Gartner E (2014) Cement and carbon emissions. *Mater Struct* 47:1055–1065
- Mikulčić H, Klemeš JJ, Vujanović M et al (2016) Reducing greenhouse gasses emissions by fostering the deployment of alternative raw materials and energy



- sources in the cleaner cement manufacturing process. *J Clean Prod* 136:119–132
9. Monteiro PJM, Miller SA, Horvath A (2017) Towards sustainable concrete. *Nat Mater* 16:698–699
 10. Pan S-Y, Chen Y-H, Fan L-S et al (2020) CO₂ mineralization and utilization by alkaline solid wastes for potential carbon reduction. *Nat Sustain* 3:399–405
 11. Juenger MCG, Siddique R (2015) Recent advances in understanding the role of supplementary cementitious materials in concrete. *Cem Concr Res* 78:71–80
 12. Wu S, Zhou J, Pan Y et al (2016) Dioxin distribution characteristics and health risk assessment in different size particles of fly ash from MSWIs in China. *Waste Manag* 50:113–120
 13. Basu M, Pande M, Bhadoria PBS, Mahapatra SC (2009) Potential fly-ash utilization in agriculture: a global review. *Prog Nat Sci* 19:1173–1186
 14. Uysal M, Akyuncu V (2012) Durability performance of concrete incorporating Class F and Class C fly ashes. *Constr Build Mater* 34:170–178
 15. Poon CS, Lam L, Wong YL (2000) A study on high strength concrete prepared with large volumes of low calcium fly ash. *Cem Concr Res* 30:447–455
 16. Langley WS, Carette GG, Malhotra VM (1989) Structural concrete incorporating high volumes of ASTM class fly ash. *Mater J* 86:507–514
 17. Babu KG, Rao GSN (1996) Efficiency of fly ash in concrete with age. *Cem Concr Res* 26:465–474
 18. Scrivener K, Martirena F, Bishnoi S, Maity S (2018) Calcined clay limestone cements (LC3). *Cem Concr Res* 114:49–56
 19. Duchesne J (2021) Alternative supplementary cementitious materials for sustainable concrete structures: a review on characterization and properties. *Waste and Biomass Valorization* 12:1219–1236
 20. Fernandez R, Martirena F, Scrivener KL (2011) The origin of the pozzolanic activity of calcined clay minerals: a comparison between kaolinite, illite and montmorillonite. *Cem Concr Res* 41:113–122
 21. Chancey RT, Stutzman P, Juenger MCG, Fowler DW (2010) Comprehensive phase characterization of crystalline and amorphous phases of a Class F fly ash. *Cem Concr Res* 40:146–156
 22. Avet F, Li X, Scrivener K (2018) Determination of the amount of reacted metakaolin in calcined clay blends. *Cem Concr Res* 106:40–48
 23. Zeng Q, Li K, Fen-chong T et al (2012) Determination of cement hydration and pozzolanic reaction extents for fly-ash cement pastes. *Constr Build Mater* 27:560–569
 24. Ben HM, De Weerd K, Lothenbach B (2010) Quantification of the degree of reaction of fly ash. *Cem Concr Res* 40:1620–1629
 25. Avet F, Scrivener K (2018) Investigation of the calcined kaolinite content on the hydration of Limestone Calcined Clay Cement (LC3). *Cem Concr Res* 107:124–135
 26. Bonavetti VL, Rahhal VF, Irassar EF (2001) Studies on the carboaluminate formation in limestone filler-blended cements. *Cem Concr Res* 31:853–859
 27. Lothenbach B, Le Saout G, Gallucci E, Scrivener K (2008) Influence of limestone on the hydration of Portland cements. *Cem Concr Res* 38:848–860. <https://doi.org/10.1016/j.cemconres.2008.01.002>
 28. Avet F, Snellings R, Diaz AA et al (2016) Development of a new rapid, relevant and reliable (R3) test method to evaluate the pozzolanic reactivity of calcined kaolinitic clays. *Cem Concr Res* 85:1–11
 29. Tazawa E, Miyazawa S (1995) Influence of cement and admixture on autogenous shrinkage of cement paste. *Cem Concr Res* 25:281–287
 30. Zhao Y, Gong J, Zhao S (2017) Experimental study on shrinkage of HPC containing fly ash and ground granulated blast-furnace slag. *Constr Build Mater* 155:145–153
 31. Jiang C, Yang Y, Wang Y et al (2014) Autogenous shrinkage of high performance concrete containing mineral admixtures under different curing temperatures. *Constr Build Mater* 61:260–269
 32. Bentz DP, Jensen OM (2004) Mitigation strategies for autogenous shrinkage cracking. *Cem Concr Compos* 26:677–685
 33. Lura P, Jensen OM, Van Breugel K (2003) Autogenous shrinkage in high-performance cement paste: an evaluation of basic mechanisms. *Cem Concr Res* 33:223–232
 34. Chang-Wen M, Qian T, Wei S, Jia-Ping L (2007) Water consumption of the early-age paste and the determination of “time-zero” of self-desiccation shrinkage. *Cem Concr Res* 37:1496–1501
 35. Tazawa E, Miyazawa S, Kasai T (1995) Chemical shrinkage and autogenous shrinkage of hydrating cement paste. *Cem Concr Res* 25:288–292
 36. Mokarem DW, Weyers RE, Lane DS (2005) Development of a shrinkage performance specifications and prediction model analysis for supplemental cementitious material concrete mixtures. *Cem Concr Res* 35:918–925
 37. Antoni M, Rossen J, Martirena F, Scrivener K (2012) Cement substitution by a combination of metakaolin and limestone. *Cem Concr Res* 42:1579–1589
 38. Medjigbodo G, Rozière E, Charrier K et al (2018) Hydration, shrinkage, and durability of ternary binders containing Portland cement, limestone filler and metakaolin. *Constr Build Mater* 183:114–126
 39. Tironi A, Scian AN, Irassar EF (2017) Blended cements with limestone filler and kaolinitic calcined clay: filler and pozzolanic effects. *J Mater Civ Eng* 29:4017116
 40. Bentz DP (2010) Powder additions to mitigate retardation in high-volume fly ash mixtures. *ACI Mater J* 107:5
 41. Ravina D, Mehta PK (1986) Properties of fresh concrete containing large amounts of fly ash. *Cem Concr Res* 16:227–238
 42. Singh M, Garg M (1999) Cementitious binder from fly ash and other industrial wastes. *Cem Concr Res* 29:309–314
 43. Dhandapani Y, Santhanam MJ (2017) Assessment of pore structure evolution in the limestone calcined clay cementitious system and its implications for performance. *Cem Concr Compos* 84:36–47
 44. Alujas A, Fernández R, Quintana R et al (2015) Pozzolanic reactivity of low grade kaolinitic clays: influence of calcination temperature and impact of calcination products on OPC hydration. *Appl Clay Sci* 108:94–101
 45. Dhandapani Y, Sakthivel T, Santhanam M et al (2018) Mechanical properties and durability performance of



- concretes with Limestone Calcined Clay Cement (LC3). *Cem Concr Res* 107:136–151
46. Ston J, Hilaire A, Scrivener K (2018) Autogenous shrinkage and creep of limestone and calcined clay based binders. In: Fernando M, Aurélie F, Karen S (eds) *Calcined clays for sustainable concrete*. Springer
 47. Khan MSH, Nguyen QD, Castel A (2020) Performance of limestone calcined clay blended cement-based concrete against carbonation. *Adv Cem Res* 32:481–491
 48. Krishnan S, Emmanuel AC, Bishnoi S (2019) Hydration and phase assemblage of ternary cements with calcined clay and limestone. *Constr Build Mater* 222:64–72
 49. Zhang Y, Afroz S, Nguyen QD et al (2021) Analytical model predicting the concrete tensile stress development in the restrained shrinkage ring test. *Constr Build Mater* 307:124930
 50. Afroz S, Nguyen QD, Zhang Y et al (2022) Evaluation of cracking potential parameters for low to high grade concrete with fly ash or slag. *Constr Build Mater* 350:128891
 51. Termkhajornkit P, Nawa T, Nakai M, Saito T (2005) Effect of fly ash on autogenous shrinkage. *Cem Concr Res* 35:473–482
 52. Chindaprasirt P, Homwuttivong S, Sirivivatnanon V (2004) Influence of fly ash fineness on strength, drying shrinkage and sulfate resistance of blended cement mortar. *Cem Concr Res* 34:1087–1092
 53. Atiş CD (2003) High-volume fly ash concrete with high strength and low drying shrinkage. *J Mater Civ Eng* 15:153–156
 54. Lee HK, Lee KM, Kim BG (2003) Autogenous shrinkage of high-performance concrete containing fly ash. *Mag Concr Res* 55:507–515
 55. Kristiawan SA, Aditya MTM (2015) Effect of high volume fly ash on shrinkage of self-compacting concrete. *Procedia Eng* 125:705–712
 56. Wongkeo W, Thongsanitgarn P, Chaipanich A (2012) Compressive strength and drying shrinkage of fly ash-bottom ash-silica fume multi-blended cement mortars. *Mater Des* 36:655–662
 57. Nguyen QD, Afroz S, Zhang Y et al (2022) Autogenous and total shrinkage of limestone calcined clay cement (LC3) concretes. *Constr Build Mater* 314:125720
 58. AS 3972 (2010) General purpose and blended cements. *Aust Stand* 1–29
 59. ASTM C618–19 (2019) Standard Specification for Coal Fly Ash and Raw or Calcined Natural Pozzolan for Use in Concrete. ASTM Int West Conshohocken, PA
 60. Afroz S, Kim T, Castel A (unpublished results) Autogenous shrinkage and microstructure of limestone calcined clay cement (LC3) paste
 61. Santana LNL, Gomes J, Menezes RR et al (2017) Microstructure development in clays upon heat treatment: Kinetics and equilibrium. *Appl Clay Sci* 135:325–332
 62. ASTM C136/C136M-19 (2019) Standard Test Method for Sieve Analysis of Fine and Coarse Aggregates. ASTM Int West Conshohocken, PA
 63. ASTM C305–20 (2020) Standard Practice for Mechanical Mixing of Hydraulic Cement Pastes and Mortars of Plastic Consistency. ASTM Int West Conshohocken, PA
 64. ASTM C1702–17 (2017) Standard Test Method for Measurement of Heat of Hydration of Hydraulic Cementitious Materials Using Isothermal Conduction Calorimetry. ASTM Int West Conshohocken, PA
 65. ASTM C1608–17 (2017) Standard Test Method for Chemical Shrinkage of Hydraulic Cement Paste. ASTM Int West Conshohocken, PA
 66. Zhang T, Gao P, Luo R et al (2013) Measurement of chemical shrinkage of cement paste: Comparison study of ASTM C 1608 and an improved method. *Constr Build Mater* 48:662–669
 67. ASTM C1698–19 (2019) Standard Test Method for Autogenous Strain of Cement Paste and Mortar. ASTM Int West Conshohocken, PA
 68. Mohr BJ, Hood KL (2010) Influence of bleed water reabsorption on cement paste autogenous deformation. *Cem Concr Res* 40:220–225
 69. Hu J, Ge Z, Wang K (2014) Influence of cement fineness and water-to-cement ratio on mortar early-age heat of hydration and set times. *Constr Build Mater* 50:657–663
 70. Snoeck D, Velasco LF, Mignon A et al (2014) The influence of different drying techniques on the water sorption properties of cement-based materials. *Cem Concr Res* 64:54–62
 71. Snellings R, Chwast J, Cizer Ö et al (2018) RILEM TC-238 SCM recommendation on hydration stoppage by solvent exchange for the study of hydrate assemblages. *Mater Struct* 51:1–4
 72. Zhang Z, Scherer GW (2021) Physical and chemical effects of isopropanol exchange in cement-based materials. *Cem Concr Res* 145:106461
 73. Zhang J, Scherer GW (2011) Comparison of methods for arresting hydration of cement. *Cem Concr Res* 41:1024–1036
 74. ASTM C109 / C109M-20b (2020) Standard Test Method for Compressive Strength of Hydraulic Cement Mortars (Using 2-in. or [50 mm] Cube Specimens). ASTM Int West Conshohocken, PA
 75. ASTM C39/C39M-21 (2021) Standard Test Method for Compressive Strength of Cylindrical Concrete Specimens. ASTM Int West Conshohocken, PA
 76. Deschner F, Winnefeld F, Lothenbach B et al (2012) Hydration of Portland cement with high replacement by siliceous fly ash. *Cem Concr Res* 42:1389–1400
 77. Li Y, Li J (2014) Capillary tension theory for prediction of early autogenous shrinkage of self-consolidating concrete. *Constr Build Mater* 53:511–516
 78. Li Y, Bao J, Guo Y (2010) The relationship between autogenous shrinkage and pore structure of cement paste with mineral admixtures. *Constr Build Mater* 24:1855–1860
 79. Ghafari E, Ghahari SA, Costa H et al (2016) Effect of supplementary cementitious materials on autogenous shrinkage of ultra-high performance concrete. *Constr Build Mater* 127:43–48
 80. Saje D (2015) Reduction of the early autogenous shrinkage of high strength concrete. *Adv Mater Sci Eng* 2015:1
 81. Berriel SS, Favier A, Domínguez ER et al (2016) Assessing the environmental and economic potential of Limestone Calcined Clay Cement in Cuba. *J Clean Prod* 124:361–369



82. Bentz DP, Ardani A, Barrett T et al (2015) Multi-scale investigation of the performance of limestone in concrete. *Constr Build Mater* 75:1–10
83. Scrivener K, Avet F, Maraghechi H et al (2018) Impacting factors and properties of limestone calcined clay cements (LC3). *Green Mater* 7:3–14
84. Du H, Dai Pang S (2020) High-performance concrete incorporating calcined kaolin clay and limestone as cement substitute. *Constr Build Mater* 264:120152
85. Hofmann MP, Young AM, Gbureck U et al (2006) FTIR-monitoring of a fast setting brushite bone cement: effect of intermediate phases. *J Mater Chem* 16:3199–3206
86. Udvardi B, Kovács JJ, Fancsik T et al (2017) Effects of particle size on the attenuated total reflection spectrum of minerals. *Appl Spectrosc* 71:1157–1168
87. Yu P, Kirkpatrick RJ, Poe B et al (1999) Structure of calcium silicate hydrate (C-S-H): Near-, Mid-, and Far-infrared spectroscopy. *J Am Ceram Soc* 82:742–748
88. Garcia-Lodeiro I, Goracci G, Dolado JS, Blanco-Varela MT (2021) Mineralogical and microstructural alterations in a portland cement paste after an accelerated decalcification process. *Cem Concr Res* 140:106312
89. Bhat PA, Debnath NC (2011) Theoretical and experimental study of structures and properties of cement paste: The nanostructural aspects of C-S-H. *J Phys Chem Solids* 72:920–933
90. Zarzuela R, Luna M, Carrascosa LM et al (2020) Producing CSH gel by reaction between silica oligomers and portlandite: a promising approach to repair cementitious materials. *Cem Concr Res* 130:106008
91. Kapeluszna E, Kotwica Ł, Różycka A, Golek Ł (2017) Incorporation of Al in CASH gels with various Ca/Si and Al/Si ratio: Microstructural and structural characteristics with DTA/TG, XRD, FTIR and TEM analysis. *Constr Build Mater* 155:643–653
92. Shi C (1998) Pozzolanic reaction and microstructure of chemical activated lime-fly ash pastes. *Mater J* 95:537–545
93. Pane I, Hansen W (2005) Investigation of blended cement hydration by isothermal calorimetry and thermal analysis. *Cem Concr Res* 35:1155–1164
94. Cho YK, Jung SH, Choi YC (2019) Effects of chemical composition of fly ash on compressive strength of fly ash cement mortar. *Constr Build Mater* 204:255–264
95. De Weerd K, Ben HM, Le Saout G et al (2011) Hydration mechanisms of ternary Portland cements containing limestone powder and fly ash. *Cem Concr Res* 41:279–291
96. Afroz S, Zhang Y, Nguyen QD et al (2022) Effect of limestone in General Purpose cement on autogenous shrinkage of high strength GGBFS concrete and pastes. *Constr Build Mater* 327:126949
97. Rostami V, Shao Y, Boyd AJ, He Z (2012) Microstructure of cement paste subject to early carbonation curing. *Cem Concr Res* 42:186–193
98. Alarcon-Ruiz L, Platret G, Massieu E, Ehrlacher A (2005) The use of thermal analysis in assessing the effect of temperature on a cement paste. *Cem Concr Res* 35:609–613
99. Kim T, Olek J (2012) Effects of sample preparation and interpretation of thermogravimetric curves on calcium hydroxide in hydrated pastes and mortars. *Transp Res Rec* 2290:10–18
100. Tazawa E, Miyazawa S (1995) Experimental study on mechanism of autogenous shrinkage of concrete. *Cem Concr Res* 25:1633–1638
101. Antiohos S, Tsimas S (2005) Investigating the role of reactive silica in the hydration mechanisms of high-calcium fly ash/cement systems. *Cem Concr Compos* 27:171–181
102. Chindaprasit P, Jaturapitakkul C, Sinsiri T (2005) Effect of fly ash fineness on compressive strength and pore size of blended cement paste. *Cem Concr Compos* 27:425–428
103. Wendner R, Hubler MH, Bažant ZP (2015) Optimization method, choice of form and uncertainty quantification of model B4 using laboratory and multi-decade bridge databases. *Mater Struct* 48:771–796
104. EN 12390-16 (2019) Testing hardened concrete - Part 16: Determination of the shrinkage of concrete. *Eur Stand*
105. AS 3600 (2018) Concrete structures. *Stand Aust*
106. Wei J, Long W-J, Khayat KH et al (2022) Dynamical properties of environmental high-performance composites with calcined clay. *J Clean Prod* 335:130226
107. Yu J, Mishra DK, Hu C et al (2021) Mechanical, environmental and economic performance of sustainable Grade 45 concrete with ultrahigh-volume Limestone-Calcined Clay (LCC). *Resour Conserv Recycl* 175:105846
108. Naseri H, Jahanbakhsh H, Hosseini P, Nejad FM (2020) Designing sustainable concrete mixture by developing a new machine learning technique. *J Clean Prod* 258:120578

Publisher's Note Springer Nature remains neutral with regard to jurisdictional claims in published maps and institutional affiliations.

